29th Congress of the International Council
of the Aeronautical Sciences
St. Petersburg, Russia; September 7–12, 2014

DEVELOPMENT OF A HYBRID ICE PROTECTION SYSTEM BASED ON NANOSTRUCTURED HYDROPHOBIC SURFACES

T. Strobl*, S. Storm*, M. Kolb*, J. Haag*, M. Hornung**
*Airbus Group Innovations, **Technical University of Munich

Abstract

Eliminating the hazard of aircraft icing still remains a challenge. Thermal-based ice protection systems are widely used to remove in-flight ice accretions. For reasons of power consumption, coatings that reduce the adhesion of the ice represent suitable approaches to protect aircraft surfaces susceptible to ice accretion. This effort intends to tailor an ultrasmooth surface with hydrophobic and icephobic properties, respectively, which are obtained by nanostructuring and subsequent surface hydrophobizing. A hybrid method of ice protection is presented in this study, where the ultrasmooth hydrophobic surface is applied on the surface of a small-scale NACA 0012 airfoil. The hybrid system further consists of a thermo-electric heater element for ice partitioning at the stagnation line by melting. Ice shedding in the unheated portion of the airfoil surface is performed by piezoelectric multilayer actuators. System performance is studied in a laboratory icing wind tunnel where it becomes evident that using the ultrasmooth, nanostructured hydrophobic surface encourages ice shedding from the airfoil surface. Measurement results also reveal that the hybrid system reduces the amount of power consumption by up to 95 % compared to state-of-the-art ice protection systems.

1 Introduction

Ice can present a hazard in a variety of day-to-day situations. In aviation, in-flight ice accretion on aerodynamic efficient surfaces such as a wing or an empennage will cause a decrease in lift, while drag is simultaneously increased [1-4]. In a worst case scenario, the handling performance of the aircraft will be lost, which might lead to fatal accidents [4]. For this purpose, ice protection systems (IPS) are used to remove the ice from critical surfaces of the aircraft during flight. The ice removal systems can be generally divided into pneumatic, chemical, thermal, and mechanical [5]. When electrically powered, the last two systems are the most promising solutions being (1) environmentally friendly, (2) energy efficient and (3) applicable within the context of an all-electric aircraft.

1.1 Paper Objectives

The first objective of the paper is to report the development a surface for reducing the adhesion between ice and solid surfaces. The surface properties of a sample aluminum alloy are tailored in such a way that the principal effects responsible for ice adhesion, namely mechanical interlocking and electrostatic adhesion, are reduced or even eliminated.

The second objective is to present a hybrid method for in-flight ice protection based on the developed surface that minimizes ice adhesion. Two additional systems will be combined for obtaining the hybridization: local heat addition using a thermal subsystem for ice partitioning at the stagnation line and mechanical surface deformation for ice shedding in the unheated aft portion of an airfoil. The deicing functionality of the hybrid method will be validated for a small-scale configuration in a laboratory-based icing wind tunnel. The aim of the study is to demonstrate that the hybrid system is able to diminish the amount of electrical power required for ice removal compared to

experimentally-obtained values reported in literature.

2 Literature Review

2.1 Superhydrophobic and Icephobic Surfaces

Different approaches for fabricating superhydrophobic and icephobic surfaces are reported in literature, with most being based on the combination of an adequately rough surface with a low-energy surface coating [6-12]. With regard to aviation applications, the increasing demand for laminar flow to reduce fuel consumption limits the degree of surface roughness, however. In addition, as ice adhesion cannot be entirely prevented, active strategies are still required to protect aircraft surfaces susceptible to ice accretion. An approach will be proposed for developing an extremely smooth surface with water and ice-repellent properties that is suited for combination with active methods of ice protection.

2.2 Thermo-electric Ice Protection Systems

When flying into atmospheric icing conditions, thermal systems are widely used throughout the aviation industry for ice protection on aircraft [5]. As state-of-the-art bleed air systems entail high fuel consumption, electro-thermal systems are well-suited for application to surfaces susceptible to ice accretion. The mode of operation can be fully-evaporative, where a large amount of power is consumed or, for reasons related to energy-efficiency, a running-wet anti-icing mode [5, 13, 14]. However, operating the system in a running-wet mode introduces the issue of runback ice. The heated area is the only region that is explicitly prevented accreting ice, while the impinging water droplets run back and freeze downstream in the unheated portion of the airfoil surface. In the context of a laminar flow wing design, any ice accretion on the wing will alter flow conditions. Hence, an electro-thermal system operated in a running-wet mode requires an add-on deicing system, like a low power consuming mechanical device to induce ice shedding.

2.3 Electro-mechanical Ice Protection Systems

The working principle of electro-mechanical deicing systems is based on the deformation of a surface affected by ice accretion. The main difference when compared to thermal methods is the fact that mechanical systems allow a certain amount of ice to be formed on the surface and the ice deposits are cyclically shed. Different implementations are used, e.g. surface deformation that is caused by high current electrical pulses delivered to electro-magnetic actuators [15]. Aspects relevant to system integration, such as electro-magnetic compatibility, are obviated as mechanical deicing systems based on piezoelectrics do not employ large currents with long rise times. Several approaches for IPS with piezoelectric actuators are reported in literature [16-18]. The challenge is, however, to design an electro-mechanical deicing system for reliable operation in each potential in-flight icing encounter, independent of environmental conditions relevant to ice accretion and independent of the thickness of the ice adhering to the aircraft surface.

2.4 Hybrid Ice Protection Systems

Hybrid IPS are able to further reduce the amount of power required to deice an aircraft. Recent studies focus on the removal of ice based on the combination of electro-thermal and electro-mechanical methods [19-22]. The thermal component of the hybrid system is set to a running-wet, anti-icing mode to prevent droplets from freezing in the area of the leading edge, while the electro-mechanical subsystem is cyclically driven for ice shedding in the unheated aft section of the airfoil [19, 20]. A similar approach for a hybrid IPS combines a periodically-driven electro-mechanical deicing system with an electric heating system in a region of an airfoil that are powered approximately simultaneously [21, 22]. The thermal subsystem is run in a deicing mode to cyclically weaken the bond between the ice and the surface of the airfoil to facilitate ice shedding through the mechanical system [21, 22]. Heat addition can also be utilized in

combination with a hydrophobic coating [23]. The adhesion between the ice and the airfoil surface is decreased due to the beneficial effect of the coating and the electrical power to run the thermal anti-ice system can likewise be reduced.

3 Methods

3.1 Description of Method

The basic idea behind the model to be developed is the reduction of power consumption by systematically combining multiple strategies for aircraft ice protection and prevention as Fig. 1 shows. The method is primarily based on the assumption that a perfectly smooth surface at the macro- and microscales, with an intentionally nanostructured surface morphology that is post-treated with a hydrophobizing agent, will minimize adhesion to such an extent that ice can be removed from the affected surface with a minimum amount of electrical power.

Surface polishing tends to eliminate any imperfections and porosities at the macro- and microscopic scales. Hence, mechanical interlocking, which is a primary mechanism of ice adhesion, can be considered negligible. Therefore, ice adhesion is reduced to a large extent [24]. A further reduction in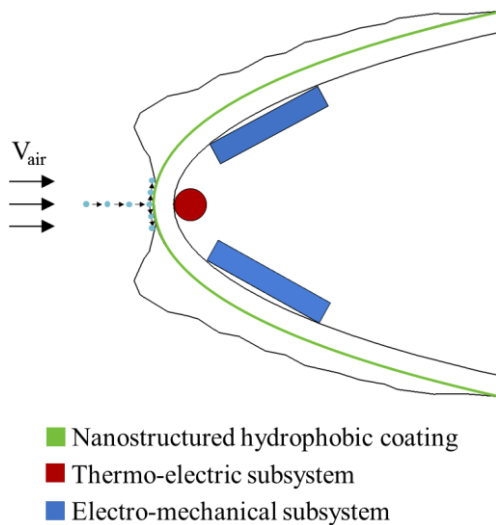 ice adhesion can be obtained if the electrostatic force of attraction between the surface and the impinging water droplets is lowered. Creating a nanoporous surface with a hydrophobizing post-treatment is a suitable means for attaining this objective [9, 12, 25, 26]. The Cassie-Baxter model [27], shown in Fig. 2, describes the idealized wetting behavior for a droplet sitting on the peaks of a sample nanotextured surface, which is covered with a thin hydrophobizing layer as shown in green. Due to the surface tension of water, the droplet does not penetrate into the cavities between the peaks. Hence, in this state, the droplet partially wets the surface and only the small part in direct contact with the peaks freezes to the surface.

The hybrid IPS, shown in Fig. 1, can be understood as the interaction produced by such a passive coating with water and ice repellent properties and a cyclically powered electro-mechanical subsystem. Since the adhesive forces between the ice and the airfoil surface are low due to its hydrophobic and icephobic character, even slight deformations of the surface in the linear elastic region will shed the ice. For ease in ice shedding, an integrated thermal method for ice prevention at the position of the stagnation line is designed to partition the ice accretion around the leading edge into upper and lower ice deposits.
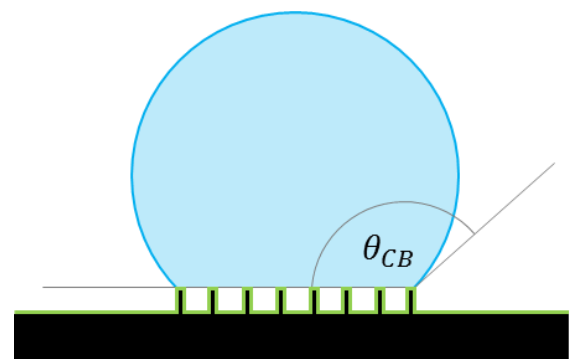

Figure 2. Wetting behavior according to the Cassie-Baxter model.

Figure 1. Working principle of the hybrid ice protection system.

3.2 Approach for Surface Tailoring

The process of tailoring an ultra-smooth surface with a nanostructured hydrophobic morphology can be divided into three steps:

(1) Mirror-polishing of aluminum alloy specimens
(2) Creation of a nanoporous aluminum oxide layer by Phosphoric Sulphuric Anodizing (PSA)
(3) Surface hydrophobizing

Flat specimens with a length of 80.0 mm and a width of 17.0 mm are cut out of bare 2024-T3 aluminum alloy sheets with thickness of 1.6 mm. After an initial surface roughness of 0.64 ± 0.03 μm is produced using an end milling cutter, the samples are polished until their surfaces get an ultra-smooth mirror finish.

Prior to anodizing, the samples are degreased in an industrially-available alkaline non-etching cleaning agent for five minutes at a temperature of 65 °C and then rinsed with deionized water for three minutes. The next step, acidic pickling, is carried out until a shiny metallic surface is achieved and again, the samples are rinsed with deionized water for three minutes. The electrochemical anodization process is carried out in an electrolyte in accordance with the Airbus technical note TN-EVC 904/96. The anodizing voltage (18 V) and the temperature (30 °C) are selected according to the PSA parameters given in Ref. [28]. In addition, two lower values of temperature (20 °C and 26 °C) and a higher magnitude of voltage (22 V) are used for the anodization process. An overview of the anodizing parameters examined within the scope of this study and the corresponding sample numbering is enumerated in Table I. For

Table I. Parameters for anodizing.

Sample No.	(a)	(b)	(c)	(d)
Voltage [V]	18	18	18	22
Temperature [°C]	20	26	30	26

all the different parameters, the thickness of the aluminum oxide layer formed during the process of anodization can be considered to be sufficient with a thickness in excess of 0.9 μm. After the anodization, the specimens are rinsed for about 10 minutes with deionized water. It is essential to mention that, for anodizing, the parameters are systematically selected to simultaneously maintain the mirror-polishing of the aluminum surface while creating a porous nanostructured aluminum surface suited for post-treatment with a hydrophobizing agent. Surface roughness is measured after the anodization as well.

To enhance the hydrophobic nature of the surface, the last step of the surface tailoring process intends to cover the peaks of the scraggy and nanoporous aluminum oxide surface obtained after anodization with a hydrophobizing agent. For this purpose, an industrially-available hydrophobizing agent of type Episurf solution of Surfactis Technologies is used in a dip-coating process according to the technical procedure for coating preparation by Surfactis Technologies [29, 30].

3.3 Design of the Hybrid Method

A key design feature of the hybrid IPS is the smooth nanostructured hydrophobic surface applied to the airfoil leading edge, which is the critical surface area for droplet impingement and freezing. For this purpose, a 177.8 mm NACA 0012 airfoil, milled out of the aluminum alloy 2024-T3, is polished until a surface with a mirror finish and no visible scratches is obtained. The airfoil is then immersed in the electrolyte according to the pre-selected anodizing parameters for surface tailoring and post-treated with the Episurf hydrophobizing agent.

Ice shedding is performed by the electro-mechanical subsystem, which is integrated inside the leading edge. Four monolithic multilayer piezoelectric actuators of type Sonox P505 of CeramTec, with a length of 30.0 mm, a width of 10.0 mm and a thickness of 2.0 mm, are therefore used. For ease in integration, a planar surface is provided at the upper and lower inner side of the leading edge.

Two actuators are attached at each location with a high-temperature epoxy adhesive film of type 3M™ Scotch-Weld™ Structural Adhesive Film AF 3109-2. Based on the inverse piezoelectric effect, application of voltage expands and contracts the actuators, and the resultant surface deformations break the bond between the ice and the surface of the airfoil.

An additional thermoelectric heater subsystem is bonded to the inside of the leading edge with the same high-temperature epoxy adhesive film as the piezoelectric actuators. The heating element, designed by QPoint Composite, is a carbon fiber cord with an active length of 90.0 mm and a diameter of 1.2 mm. For electrical insulation from the metallic airfoil, the carbon heater provides thin layers of glass fiber wrapped around the carbon fibers and the whole composite is infiltrated with epoxy resin. It was noted that the carbon heater is not intended for large-scale heat addition to melt the ice in regions of the leading edge impingement area [19-22], but only local heat addition at the stagnation line. The ice accretion is thereby divided into an upper and lower part, which is compulsory for the proposed functionality of the electro-mechanical subsystem. Without the insertion of a predetermined breaking point, the continuous ice accumulation around the leading edge remains in the same position though the ice is mechanically released from the airfoil surface, since the aerodynamic forces press the ice against the airfoil [16].

3.4 Setup for System Performance Testing

Prior to testing the deicing performance of the hybrid IPS, samples (a) to (d) are evaluated regarding their potential to reduce ice adhesion. Therefore, a thin layer of glaze ice is accreted on the samples using the laboratory icing wind tunnel facility of Airbus Group Innovations (formerly EADS Innovation Works) [24]. The conditions selected for ice accretion are the same as in Ref. [24]. The test setup includes a permanent magnet shaker and measurement equipment to determine the degree of icephobicity of each sample and, more specifically, to select the most promising

approach among these samples for application to the hybrid ice protection system [24].

Validation of the hybrid method and, in particular, the interaction between the nanostructured hydrophobic surface and the internally integrated thermo-electric and electro-mechanical components is also performed in the icing wind tunnel of Airbus Group Innovations [24]. The airfoil with the integrated hybrid system is mounted in the test section at zero degree angle of attack. Power supplies of type EA-PSI 8720-15 are used for the thermo-electric subsystem with the carbon heater and also the electro-mechanical subsystem. For reasons of power amplification, a MAC audio amplifier of type MPX 4500 is required for the piezoelectric multilayer actuators. The excitation signal for the actuators is provided by a dynamic signal analyzer of type Agilent 35670A. Prior to testing the system functionality in the icing wind tunnel, the analyzer is also used to characterize the airfoil with the integrated hybrid ice protection system regarding its resonance behavior.

Icing conditions typical for glaze ice shapes are investigated, in which three test runs are carried out. The static air temperatures (T_{st}) and total air temperatures (T_{tot}) of the test runs are listed in Table II. The target velocity of the airstream (V_{air}) for performing the experimental investigations is 120.0 m/s. The actual values of V_{air} are shown in Table II. Supercooled water droplets with a median volume diameter (MVD) of 20.0 µm are supplied by a spray bar system, which is installed in the settling chamber of the icing wind tunnel [24]. The liquid water content (LWC), is set equal to 0.45 g/m³ according to the continuous maximum intensity of atmospheric icing conditions (CS-25 Appendix C icing conditions) [31]. When the total air temperature in the test section is stable, atomization of

Table II. Icing wind tunnel tests of the hybrid method.

Test run	T_{st} [°C]	T_{tot} [°C]	V_{air} [m/s]
1	-7.8	-0.8	118.9
2	-8.4	-1.2	120.1
3	-7.9	-0.9	118.7

supercooled water droplets is initiated. While the spray system is activated, the thermal subsystem works in a running-wet anti-icing mode to permanently keep the stagnation line free from ice and the ice accumulating in the unheated portions of the airfoil is cyclically shed by the piezoelectric actuators.

4 Results

4.1 Evaluation of Surface Tailoring

Maintaining the ultra-smooth mirror-polished surface finish is deemed essential throughout the process of tailoring a surface with water and icephobic properties. Macroscopic and microscopic evaluation of the surface is therefore carried out before and after anodizing, where the electrolyte chemically modifies the surface. Roughness measurements are taken with a DektakXT perthometer of Bruker according to DIN EN ISO 4288:1998 and DIN EN ISO 3274:1998. After polishing, the arithmetic mean value of surface roughness (R_a) is equal to 0.02 ± 0.002 µm. Table III shows the values of R_a for the samples (a) to (d) after the anodizing. It becomes evident that specimen (a) still provides the same value of surface roughness with R_a equal to 0.02 ± 0.002 µm. Raising the temperature of the electrolyte up to 26 °C and 30 °C for samples (b) and (c), respectively, or increasing the magnitude of anodizing voltage up to 22 V for sample (d), leads to a slight increase in the surface roughness for the three samples as depicted in Table III.

To evaluate the potential of a surface regarding its wetting behavior and, in particular, its hydrophobic or even superhydrophobic character, contact angle measurements with water can be considered an adequate means. However, measuring the contact angle hysteresis (CAH) is more appropriate to evaluate the degree of icephobicity [32-34]. The value of CAH is defined as the difference between the advancing contact angle (CAA) and the receding contact angle (CAR). A Krüss contact angle measuring system G10 equipped with a 6.4 mm x 4.8 mm CCD Camera is used. Table III lists the values of CAA, CAR and CAH determined for the samples (a) to (d). Since all the specimens are immersed in the same Episurf solution, the reasons for the variation in the contact angles are due to the anodizing parameters, i.e. the formation of the aluminum oxide layer obtained by anodization is a function of the electrolyte temperature and the magnitude of anodizing voltage. Considering first an anodizing voltage of 18 V, the evolution of the pore size as a function of the electrolyte temperature is illustrated in the SEM topography images in Fig. 3 a) to c). As shown in Fig. 3 a), the surface porosity of the aluminum sample immersed in the electrolyte at room temperature (20 °C) can be considered to be rather poor and, after hydrophobization with the Episurf solution, the resulting measurement values of CAA, CAR and CAH with 151.5 °, 136.3 °, and 15.2 °, respectively, reinforce this fact. The increase in temperature of the electrolyte for sample b) up to 26 °C leads to a fluffy nanoporous surface morphology as shown in Fig. 3 b). This is due to the enhanced chemical reaction rate and the resultant increase in the dissolving capacity. The measurements listed in Table III reveal that

Table III. Effects of temperature and voltage variation while anodizing.

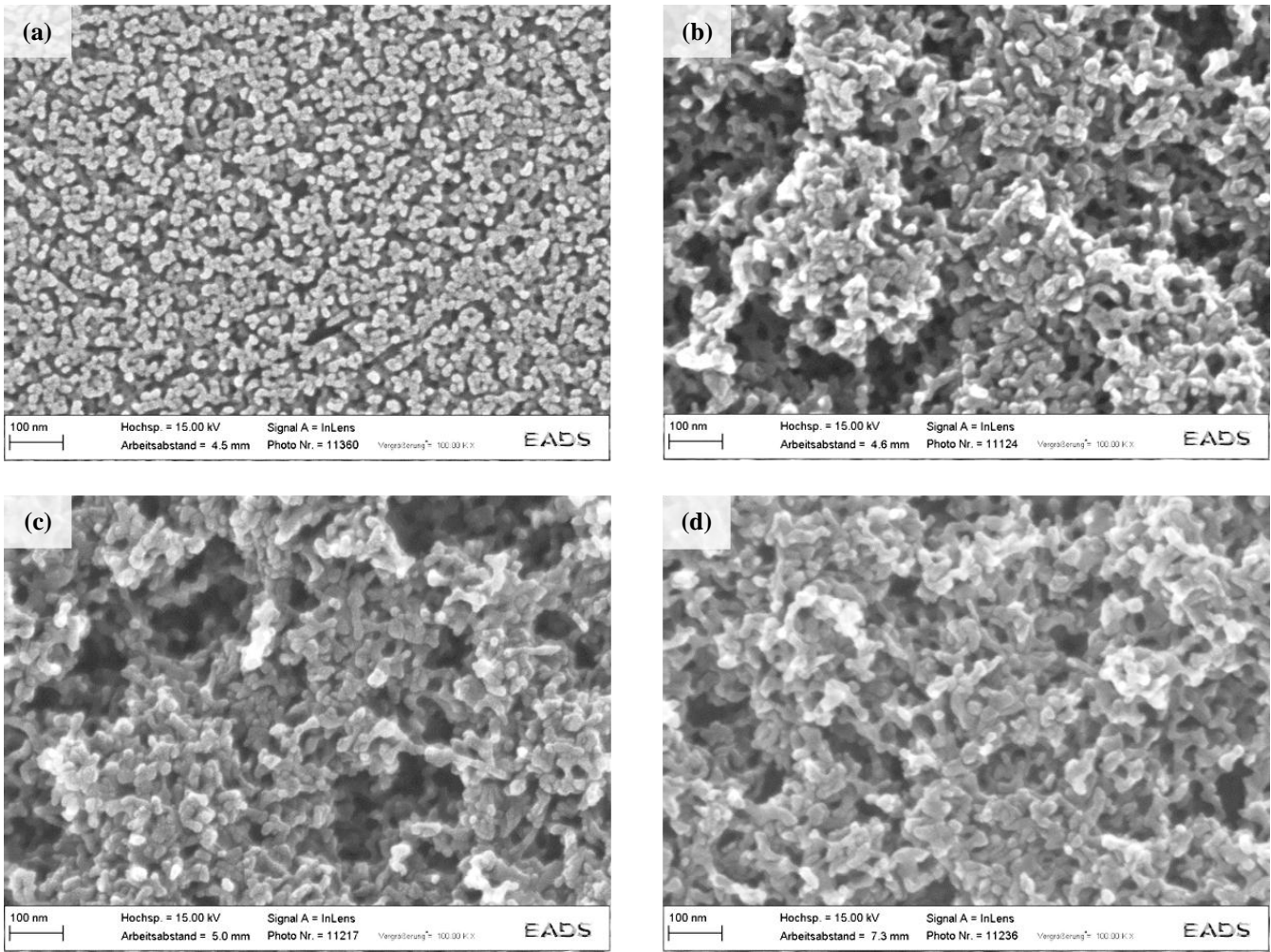| Sample No.	(a)	(b)	(c)	(d)
R_a [µm]	0.020 ± 0.002	0.073 ± 0.005	0.077 ± 0.005	0.070 ± 0.007
CAA [°]	151.5 ± 1.21	160.6 ± 0.59	158.6 ± 0.56	160.0 ± 0.37
CAR [°]	136.3 ± 1.48	158.1 ± 0.14	155.8 ± 0.21	156.5 ± 0.47
CAH [°]	15.2	2.5	2.9	3.5

Figure 3. Top-view SEM images of the anodized samples at (a) 18 V/20 °C, (b) 18 V/26 °C, (c) 18 V/30 °C, and (d) 22 V/26 °C

sample b) shows the best performance in terms of icephobicity with a CAA of 160.6 ± 0.59 °, a CAR of 158.1 ± 0.14 °, and thus a CAH of 2.5 °. This can be explained by the low nanopore density obtained for sample b). With a further increase in the electrolyte temperature up to 30 °C, as employed in the production of sample c), an enhancement of the dissolving capacity is observed. The corresponding top-view SEM image shown in Fig. 3 c) indicates that the increase in temperature affects the surface morphology in such a way that the density of the nanopores increases and the pores themselves seem to become overgrown. Regarding the degree of hydrophobicity and icephobicity, respectively, sample (c) shows lower values of CAA, CAR and CAH with 158.6 ± 0.56 °, 155.8 ± 0.21 °, and 2.9 ° compared to sample (b). The effect of voltage

variation on the nanostructure becomes evident by comparing samples (b) and (d), both immersed in the electrolyte with a temperature of 26 °C. The increase in the anodizing voltage by 4 V for sample (d) accelerates the formation of the aluminum oxide layer, which increases the nanopore density as depicted in the SEM image in Fig. 3 d). The measured values of CAA, CAR and CAH with 160.0 ± 0.37 °, 156.5 ± 0.47 °, and 3.5 °, respectively, indicate that the degree of icephobicity is slightly lower for sample (d) when compared to sample (b).

The quantification of ice adhesion strength, performed using the permanent magnet shaker, is shown in Fig. 4 for the samples (a) to (d). The measured values of interfacial adhesion strength (τ_{int_adh}), which are required to release the ice from the respective sample surface, are depicted as a function of the contact angle hysteresis. The
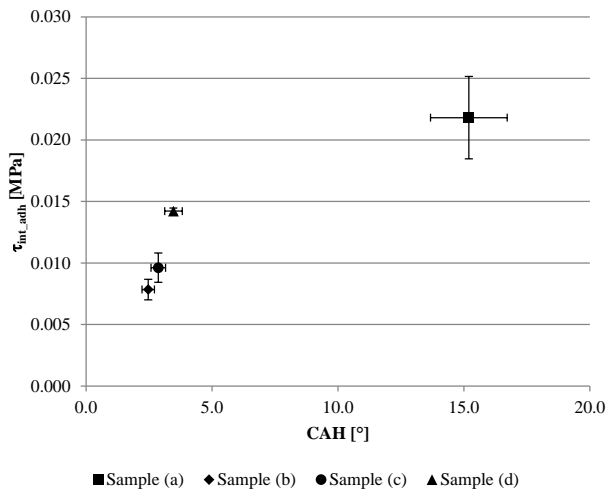
Figure 4. Evaluation of ice adhesion.

lowest magnitude of ice adhesion is obtained for sample (b) with a required value of τ_{int_adh} of 0.008 ± 0.001 MPa. Comparing the results of τ_{int_adh} to the values of CAH, it becomes evident that both measuring techniques reveal the same sample ranking: (a) > (d) > (c) > (b), with (a) showing the worst and (b) showing the best performance.

In a nutshell, the anodizing parameters of sample (b), selected to fabricate a nanoporous surface morphology, provide an optimum pore size and arrangement and, more importantly, the best potential for being combined with a hydrophobizing agent for reasons of low ice adhesion properties.

4.2 Validation of the Hybrid Method

Based on the results of the parameter study for anodization, the leading edge of the airfoil has been immersed in the electrolyte using the same process parameters as sample (b). Fig. 5 shows the NACA 0012 airfoil with the nanostructured

Figure 5. NACA 0012 airfoil with the ultrasmooth nanostructured hydrophobic surface in the leading edge area.

hydrophobic surface prior to the installation of the electrical components of the hybrid system. It becomes evident that the scraggy nanostructured surface obtained by anodizing does not affect the mirror-polished appearance of the surface.

Prior to validating the functionality of the hybrid method under icing conditions, the entire system, i.e. the airfoil, the carbon heater and the piezoelectric actuators, but without ice accretion on the surface of the airfoil, is analyzed using the dynamic signal analyzer. A frequency sweep from 500 Hz to 50 kHz is employed. The behavior of the resonant system is described by its reactance as shown in Fig. 6. The progressions of the amplitude and the phase of the reactance are a function of the excitation frequency of the system. The peak in the phase progression at -73.8 ° corresponds to a frequency of approximately 4.25 kHz. This data point is taken to be the reference stimulus value, since the resonance of the system, i.e. the maximum displacement of the airfoil surface, is obtained at this point. Fig. 7 shows the progressions of the real and complex powers measured for simultaneous operation of all the four piezoelectric actuators. For the maximum deformation of the surface at the reference stimulus value of 4.25 kHz, a required value of real power of 4.47 W has to be provided when using a Class D audio amplifier with 95 % efficiency as power input.

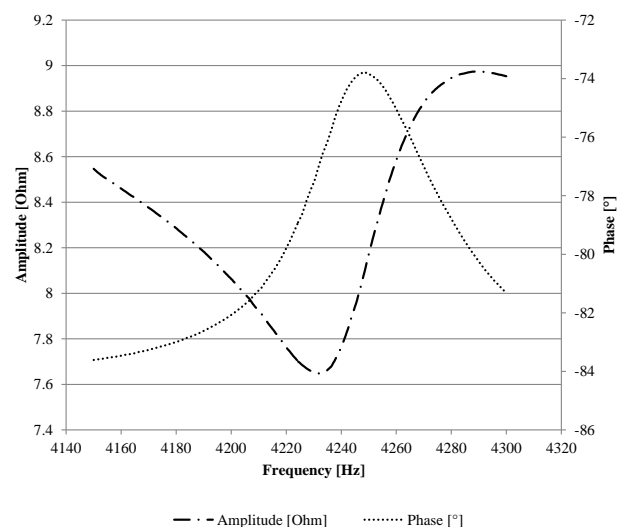For testing the system performance and the

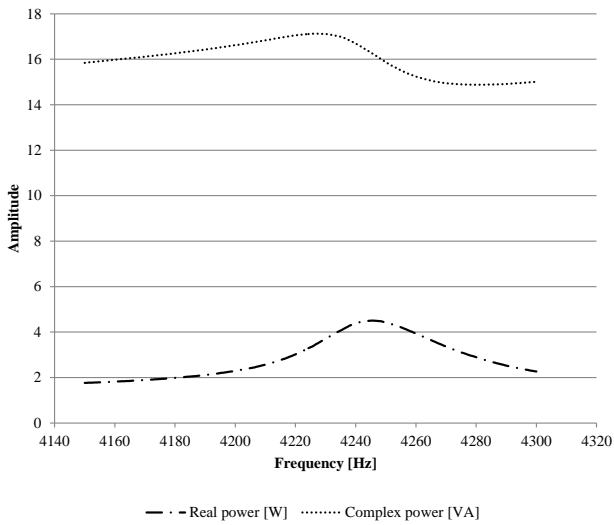Figure 6. Reactance of the hybrid ice protection system.

Figure 7. Power consumption of the hybrid ice protection system.

deicing capability in the icing wind tunnel, a sweep around the reference stimulus value over a frequency range from 4.15 kHz to 4.30 kHz is employed. Since the resonance of the system might be shifted due to the damping effect of ice formations on the airfoil surface, and also by slight variations in the ambient temperature where icing tends to occur, the frequency sweep ensures that the resonant frequency of the airfoil structure is applied for each possible ice shape and thickness. The cycle duration of the sweep excitation is arbitrarily set equal to 2 s.

Fig. 8 shows a sample glaze ice accretion, which is shed from the airfoil surface as illustrated in the 8 consecutive images over a total time interval of 0.0175 s. The deicing sequence is shot with a Phantom® v611 high speed camera with 400 frames per second. The first image visualizes ice partitioning, which results from heat addition to the stagnation line by the carbon fiber cord. Aft of the heated area, ice accretes on the upper and lower portions of the airfoil surface. It is essential to notice that, at this particular time, the piezoelectric actuators are still deactivated. As soon as power is supplied to the actuators, the surface of the airfoil starts to deform as in the second image of the sequence. When it comes to excitation at the resonance frequency of the structure, maximum surface deformation is obtained and the ice is shed as in the third shot. The remaining 5 images visualize how the shed ice fragments are carried away by the airstream.

The total power density (p_{d_tot}) of the hybrid system is composed of the heater power and the piezoelectric portion of power, both in reference to the surface area affected by the ice formation (A_{surf_ice}):

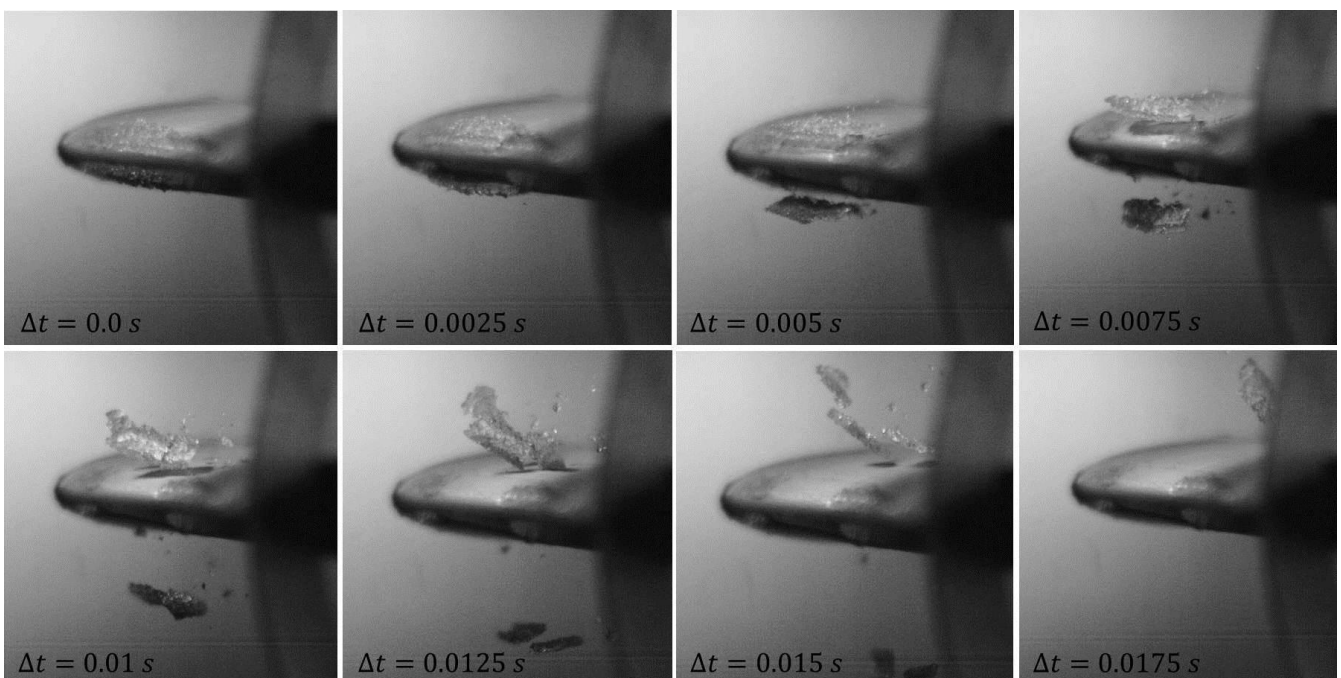$$p_{d\_tot} = \frac{P_{CFC} + P_{PZT}}{A_{surf\_ice}} \qquad (1)$$

Figure 8. Deicing sequence of a sample glaze icing condition shot with a high speed camera.

where P is the variable for the electrical power and the subscripts CFC and PZT stand for the carbon fiber cord heater and the piezoelectric actuators, respectively. Note that the dimensions of A_{surf_ice} in Eq. (1) are determined without powering the carbon fiber cord and the piezoelectric actuators. For the conditions given in Table II, the ice accretion extends along the entire span of the airfoil (100 mm in length), and with a wrap distance of approximately 40 mm in the chordwise direction. Thus, the surface area of the airfoil, which is covered with ice, amounts to approximately 0.004 m².

Throughout the three test runs listed in Table II, the carbon fiber cord has to be powered with a 7.0 V input voltage and a current of 0.8 A to keep the stagnation line free from ice. This yields a heater power of 5.6 W. The piezoelectric portion of the total power density in Eq. (1) refers to the measurement without ice accretion. This assumption is valid as each slight variation in the ice shape and, in particular, the ice thickness, will alter the damping behavior and the resonance frequency of the system to a certain extent, but the magnitude of voltage and current required to mechanically break away the ice from the airfoil surface will not be affected. Note that, due to the general characteristics of piezoelectric elements, a conservative assumption using a measurement deviation of 20 % is made. Hence, with the measured value of real power equal to 4.47 W as shown in Fig. 7, the maximum piezoelectric power is 5.36 W. Substituting all the values in Eq. (1) yields a total power density of 2.74 kW/m² for the hybrid ice protection system.

4.3 Discussion

The potential of this hybrid system to reduce power consumption for aircraft deicing applications becomes apparent when considering the amount of power consumed by state-of-the art systems certified for flight in icing conditions, e.g. strictly thermal ice protection systems with power densities in the range between 16.4 kW/m² and 62.0 kW/m² [7]. The energy-efficiency of the proof-of-concept hybrid IPS is further emphasized by the fact that the electro-mechanical subsystem with the

piezoelectric multilayer actuators can be operated at a very low value of power density, which is approximately 57 % less the power density of a competing electro-mechanical subsystem [21]. In addition, the thermal power density for the hybrid method developed is approximately one fortieth of the value given in literature [13].

In addition to the aspect of energy-efficiency, the electro-thermal and -mechanical components of the hybrid method reduce weight, as the linear heat addition for ice partitioning at the stagnation line by means of the carbon fiber cord replaces a heavier large-scale heater system for melting the ice in the entire droplet impingement area on the leading edge. The piezoelectric actuators and the carbon heater are also suited to be used for deicing applications with the additional constraint of space limitations. Further, structural integration of the components in the leading edge of the airfoil requires no moving parts and, therefore, a high life expectancy can be anticipated.

5 Conclusion

An ultra-smooth nanostructured surface with hydrophobic and icephobic properties is developed in this study. Based on the results of surface tailoring, a hybrid method for ice protection is proposed. The approach of the hybridization is based on the idea of combining the water and ice repellent surface with multiple strategies of ice removal, primarily for reasons related to energy reduction. Systematic heat addition prevents ice from accreting on the airfoil stagnation line, while the ice accreting in the unheated upper and lower areas on the airfoil surface is shed via an electro-mechanical subsystem that employs piezoelectric actuators. The reduction in power consumption of the hybrid IPS amounts up to 95 % relative to state-of-the art IPS.

Acknowledgments

wind tunnel staff and other Airbus Group Innovations engineering staff.

References

[1] Civil Aviation Authority. (2000, June 14). Aircraft Icing Handbook. Retrieved April 09, 2011, from http://www.caa.govt.nz/search/query.asp.

[2] Federal Aviation Administration. (2007, December 31). Advisory Circular AC 91-74A - Pilot Guide: Flight in Icing Conditions. Retrieved April 09, 2011, from http://rgl.faa.gov/REGULATORY_AND_GUIDANCE_LIBRARY%5CRGADVISORYCIRCULAR.NSF/0/4C8192BB0B733862862573D2005E7151?OpenDocument.

[3] Airbus Industrie (2000). Getting to Grips with Cold Weather Conditions. A Flight Operations View; Flight Operations Support - Customer Services Directorate. AI/ST-F 945.9843/99. Ref: AI/SR A007-01/00.

[4] K.R. Petty, C.D.J. Floyd, A STATISTICAL REVIEW OF AVIATION AIRFRAME ICING ACCIDENTS IN THE U.S.

[5] Alegre, N., Full-Scale Runback Ice: Accretion and Aerodynamic Study, https://dspace.lib.cranfield.ac.uk/bitstream/1826/5547/1/Nathalie_Alegre_Thesis_2010.pdf.

[6] R. Jafari, R. Menini, M. Farzaneh, Superhydrophobic and icephobic surfaces prepared by RF-sputtered polytetrafluoroethylene coatings, Applied Surface Science 257 (2010) 1540–1543.

[7] E. Celia, T. Darmanin, E. Taffin de Givenchy, S. Amigoni, F. Guittard, Recent advances in designing superhydrophobic surfaces, Journal of Colloid and Interface Science 402 (2013) 1–18.

[8] R. Menini, M. Farzaneh, Advanced Icephobic Coatings, Journal of Adhesion Science and Technology 25 (2011) 971–992.

[9] S. Farhadi, M. Farzaneh, S. Simard, On Stability and Ice-Releasing Performance of Nanostructured Fluoro-Alkylsilane-Based Superhydrophobic Al alloy2024 Surfaces, International Journal of Theoretical and Applied Nanotechnology 1 (2012) 38–44.

[10] D.K. Sarkar, M. Farzaneh, Superhydrophobic Coatings with Reduced Ice Adhesion, Journal of Adhesion Science and Technology 23 (2009) 1215–1237.

[11] F. Arianpour, Water and ice-repellent properties of nanocomposite coatings based on silicone rubber: Propriétés hydrophobes et galciophobes de revêtements nanocomposites à base de silicone, Library and Archives Canada = Bibliothèque et Archives Canada, Ottawa, 2011.

[12] F. Arianpour, M. Farzaneh, On Hydrophobic and Icephobic Properties of TiO2-Doped Silicon Rubber Coatings, International Journal of Theoretical and Applied Nanotechnology 1 (2012) 79–85.

[13] K. Al-Khalil, Effect of Mixed Icing Conditions on Thermal Ice Protection Systems, [April 15, 2013], http://www.coxandco.com/files/pdf/FAA-D9688.pdf.

[14] K. Al-Khalil, E. Irani, Mixed Phase Icing Simulation and Testing at the Cox Icing Wind Tunnel, AIAA-2003-0903 2003, 6 January 2003.

[15] Cox & Company Inc., Low Power Ice Protection Systems, [April 15, 2013], http://www.coxandco.com/products/low_power_ice_protection_systems.html.

[16] S. Struggl, J. Korak, C. Feyrer, M. Tomizuka, SPIE Proceedings, pp. 79815L.

[17] A. Overmeyer, J. Palacios, E. Smith, R. Royer, Rotating Testing of a Low-Power, Non-Thermal Ultrasonic De-icing System for Helicopter Rotor Blades, SAE Technical Paper 2011-38-0098, 2011, doi 38 (2011).

[18] S.V. Venna, Y.-J. Lin, G. Botura, Piezoelectric Transducer Actuated Leading Edge De-Icing with Simultaneous Shear and Impulse Forces, JOURNAL OF AIRCRAFT 44 (2007) 509–515.

[19] K. Al-Khalil, T. Ferguson, D. Phillips, A Hybrid Anti-icing Ice Protection System, AIAA 97-0302 (1997).

[20] K. Al-Khalil, T. Ferguson, Cox & Company, Inc., U.S. Patent Application for a "Hybrid ice protection system for use on roughness-sensitive airfoils", Docket No. US 09/330,444, filed 19 Jun. 1996.

[21] K. Al-Khalil, Thermo-Mechanical Expulsion Deicing System - TMEDS, [April 15, 2013], http://www.coxandco.com/files/pdf/AIAA-2007-0692.pdf.

[22] K. Al-Khalil, Cox & Company, Inc., U.S. Patent Application for a "Energy-efficient electro-thermal and electro-mechanical ice-protection method", Docket No. US 12/323,685, filed 26 Nov. 2008.

[23] G. Fortin, M. Adomou, J. Perron, Experimental study of hybrid anti-icing systems combining thermoelectric and hydrophobic coatings, SAE International, Warrendale, Pa, 2011.

[24] T. Strobl, D. Raps, M. Hornung, Evaluation of Roughness Effects on Ice Adhesion, in: 5th AIAA Atmospheric and Space Environments Conference, American Institute of Aeronautics and Astronautics, 2013.

[25] V. Bahadur, L. Mishchenko, B. Hatton, J.A. Taylor, J. Aizenberg, T. Krupenkin, Predictive Model for Ice Formation on Superhydrophobic Surfaces, Langmuir 27 (2011) 14143–14150.

[26] A.J. Meuler, J.D. Smith, K.K. Varanasi, J.M. Mabry, G.H. McKinley, R.E. Cohen, Relationships between Water Wettability and Ice Adhesion, ACS Appl. Mater. Interfaces 2 (2010) 3100–3110.

[27] A.B.D. Cassie, S. Baxter, Wettability of porous surfaces, Trans. Faraday Soc. 40 (1944) 546.

[28] F. Museux, R. Theilmann, FAST - Flight Airworthiness Support Technology: Introducing more eco-efficient chemical treatments for aircraft structure, Towards a chromate-free Airbus, [February

20, 2014],
http://www.airbus.com/support/publications/?eID=dam_frontend_push&docID=17481.

[29] Surfactis Technologies, EPISURF solution preparation and surface treatment: TECHNICAL PROCEDURE. RD_120612_v01, 2012.

[30] Surfactis Technologies, EPISURF solution preparation and surface treatment: TECHNICAL PROCEDURE (TP), COMPOUND 08-202. RD_020909_v02, 2012.

[31] Certification Specifications for Large Aeroplanes CS-25 - Flight in Icing Conditions, European Aviation Safety Agency.

[32] C.W. Extrand, Model for Contact Angles and Hysteresis on Rough and Ultraphobic Surfaces, Langmuir 18 (2002) 7991–7999.

[33] C.W. Extrand, Designing for Optimum Liquid Repellency, Langmuir 22 (2006) 1711–1714.

[34] K.M. Smyth, Wetting hysteresis and droplet roll off behavior on superhydrophobic surfaces / by Katherine Marie Smyth, 2010.

Contact Author Email Address

Tobias.Strobl@eads.net
Stefan.Storm@eads.net
Max.Kolb@eads.net
Jana.Haag@eads.net
Mirko.Hornung@tum.de

Copyright Statement